Differential Protection Algorithm Founded on Kalman Filter Based Phase Tracking

Differential Protection Algorithm Founded on Kalman Filter-Based Phase Tracking

Mohsen Tajdinian, Haidar Samet, *Member, IEEE*, and Ziad M. Ali

***Abstract*— Owing to the large magnitude of the inrush currents, the functionality of differential protection of power transformer may be threatened in correct discrimination between inrush and internal faults. This article enhances the functionality of differential protection through a computationally efficient method that utilizes the phase angle current signals of the current transformers (CTs). The proposed discrimination criterion (PDC) tracks the fundamental phase angle of the current signals of the CTs. While during an internal fault, the phase angles of both CTs are almost constant and in phase, during the external fault and inrush currents, the phase angles of both CTs have notable distance. On this ground, this article employs a developed Kalman filter (KF)-based phase angle estimator to measure the fundamental phase angles of the current signals of the CTs. Afterward, PDC is introduced that measures the distance between the estimated phase angles of the CT's currents. Evaluating the effectiveness of the PDC with several simulated and experimental recorded current signals reveals the PDC is able to detect internal faults even in the presence of CT saturation and also to deal with inrush and external fault currents.**

***Index Terms*— Differential protection, magnetization current, power transformer.**

I. Introduction

A POWER transformer is considered as one of the most strategic and vital components in the power system. Due to the importance of power transformers' operation for system reliability and power delivery continuity, differential protection schemes are widely employed to decrease the damages caused by internal faults [1]. The differential relay operates based on differential currents and due to the power transformer core nonlinearity, large currents may lead differential protection to maloperation under magnetization inrush currents. The harmonic restrain algorithm is known as the most famous differential protection algorithm that utilizes the harmonic contents of the current signals to discriminate between internal faults and inrush currents [1], [2]. Employing low-loss material in the transformer's core has led to the production of magnetization inrush currents with lower second harmonic contents [3]. Besides, transformer energization with internal fault, internal fault under current transformer (CT) deep saturation, and transformer energization with high remnant flux are the issues that significantly affect the harmonic contents and consequently, the performance of the harmonic restrain algorithm and differential relays. Note that due to the essence of the accuracy of measurement in protective relays, closed-loop iron-core CTs are utilized for protection applications. However, it has been acknowledged that such a type of CT experiences saturation which leads to waveform deformation. Obviously, measurement algorithms in protective relays are profoundly affected by the latter waveform deformations [3]. It is worth mentioning that several research studies have been dedicated to providing different structures for CTs to enhance the accuracy and consequently to reduce the impact of waveform deformations on protective relays [4]–[6].

To deal with internal faults and inrush current discrimination, several algorithms have been proposed in the literature that tried to introduce signal processing techniques to tackle the aforementioned challenges. These algorithms are divided into five groups including the following:

1) G1: harmonic restraint [1], [2];
2) G2: induced voltage, flux linkage, and instantaneous inductance [8], [9];
3) G3: pattern recognition, artificial intelligence, and fuzzy logic [10]–[14];
4) G4: time–frequency analysis [15]–[19];
5) G5: ratio-based algorithms [20]–[22];
6) G6: statistical and similarity indices [23]–[27].

More or less, these methods have successfully dealt with some of the challenges. However, some restrictions and computationally ineffectiveness of most of these algorithms make them vulnerable and incomprehensive regarding all difficult scenarios. According to Table I, we have the following explanation.

The methods in (G1) [1], [2] operate based on the harmonic content of the differential current. More specifically, during transformer energization, due to the core's nonlinearity, the power transformer draws a large current known as inrush current. It has been acknowledged that due to nonlinear B–H characteristics of the transformer's core, the inrush current contains notable second-order harmonic currents and as a

Manuscript received September 23, 2021; revised November 13, 2021; accepted December 10, 2021. Date of publication December 22, 2021; date of current version March 1, 2022. The Associate Editor coordinating the review process was Guglielmo Frigo. *(Corresponding author: Haidar Samet.)*

Mohsen Tajdinian is with the Department of Power and Control, School of Electrical and Computer Engineering, Shiraz University, Shiraz 7134851154, Iran (e-mail: tajdinian.m@shirazu.ac.ir).

Haidar Samet is with the Department of Electrical Engineering, Eindhoven University of Technology, 5612 AZ Eindhoven, The Netherlands, and also with the Department of Power and Control, School of Electrical and Computer Engineering, Shiraz University, Shiraz 7134851154, Iran (e-mail: samet@shirazu.ac.ir).

Ziad M. Ali is with the College of Engineering at Wadi Addawasir, Prince Sattam Bin Abdulaziz University, Al-Kharj 11991, Saudi Arabia, and also with the Electrical Engineering Department, Faculty of Engineering, Aswan University, Aswan 81542, Egypt (e-mail: dr.ziad.elhalwany@aswu.edu.eg).

Digital Object Identifier 10.1109/TIM.2021.3137565

TABLE I
COMPARISON BETWEEN DIFFERENT GROUPS OF APPROACHES

Group	Data Requirement	Extra Device Requirement	Computational Burden	Noise Sensitivity	CT Saturation
G1	1 Cycle	No	Moderate	Low	Venerable
G2	Up to 1 Cycle	Yes	High	Low	Relatively Immune
G3	Up to 1 Cycle	No	Very High	Moderate	Relatively Immune
G4	Up to 1 Cycle	No	Moderate	Very High	Relatively Immune
G5	1 Cycle	Yes	Moderate	Moderate	Immune
G6	Up to 1 Cycle	No	Relatively Low	Moderate	Immune

result, the magnetic flux in the core is not sinusoidal and the transformer generates harmonics. Although these algorithms have acceptable noise sensitivity, they require one cycle of data and also fail during fault conditions accompanied by CT saturation. Moreover, by utilizing low-loss materials in the transformer's core, the second harmonic content of the magnetization inrush currents may reduce which may result in the maloperation of the harmonic restrain algorithm.

The methods in (G2) [8], [9] calculate the induced voltage, flux linkage, and instantaneous inductance, and are thus dependent on transformer parameters and require extra accessories such as search coil that make these methods costly.

On the other hand, the methods in (G3) [10]–[14] require high memory and training data and also impose a high computational burden if they are to provide good performance.

Being sensitive to noise and requiring a high sampling rate are the drawbacks of the algorithms in (G4) [15]–[19].

The algorithms in (G5) [20]–[22] employ voltage signals as auxiliary information, meaning that these approaches particularly require two potential transformers for implementation. Moreover, these algorithms conduct the calculation based on the discrete Fourier transform that imposes an inherent one-cycle delay to the algorithm.

Eventually, the algorithms in (G6) [23]–[27] utilize some characteristics of the signal to find the similarity/dissimilarity of the signal to a standard sinusoidal waveform. It is obvious that these algorithms may show vulnerability and sensitivity to the decaying dc and noise components and also deep CT saturation conditions.

This article tries to enhance the reliability of the power transformer differential protection to reduce the malfunctioning during inrush currents. To such an aim, this article introduces a combined method that employs the phase angles of the CTs currents. The proposed algorithm provides the following contributions.

1) The proposed algorithm employs a fast phase angle estimator based on the Kalman filter (KF). Due to the recursive nature of the Kalman filter, the presented estimator does not require a high sampling rate.
2) To discriminate the internal faults from other disturbances, the proposed discrimination criterion (PDC) calculates the distance between phase angles of the current signals of the CTs. The PDC distinguishes the internal faults from the inrush current and the external fault signals considering the fact that during an internal fault, the phase angles of both CTs are almost constant and in phase, during the external fault and inrush currents, the phase angles of the both CTs have notable distance. Note that the fundamental phase angle of a fault signal remains almost constant during the fault since the fault current is almost fit on a sinusoidal waveform. However, the inrush current does not fit on a sinusoidal waveform and as a result, the phase angle varies. Also, considering current flow during the internal and external fault, during the internal fault, the phase angles of the current signals of CTs are in phase while during the external fault, the phase angles of the current signals of CTs are 180° out of phase. As a result, the PDC can comprehensively deal with different inrush and fault circumstances.
3) Due to fast phase angle estimation, the PDC has immunity to the internal and external faults accompanied by heavy CT saturation.
4) The simple definition of PDC in combination with the recursive nature of the Kalman filter makes the proposed method computationally efficient.

Section II discusses the mathematical basis of the proposed algorithm including the Kalman filter and PDC. Section III provides the implementation steps of the proposed index. Section IV is dedicated to performance evaluation and result discussion. Finally, Section V is dedicated to discussions regarding the conclusion.

II. PROPOSED ALGORITHM

The proposed method is designed based on the distance of the phase angles of the CT's current signals. As a result, it is first required to calculate the phase angle from the CT's current signals. The current signal at kth sample is expressed as follows:

$$i_{\mathrm{ct}}(k) = I_{\mathrm{m}} \cos(2\pi f_0 k T_{\mathrm{s}} + \delta) + \varepsilon_k \tag{1}$$

where I_{m} and δ show the magnitude and phase angle of the fundamental component. Also f_0, Δf, T_{s}, and ε_k denote the nominal frequency, frequency deviation, and sampling time, noise, respectively. To construct complex expression of the current signal and by using signal phase shifting, the following can be obtained:

$$\begin{aligned} i(k) &= i_{\mathrm{ct}}(k) + j i_{\mathrm{ct}}\left(k - \frac{N}{4}\right) \\ &= I_{\mathrm{m}} e^{j(2\pi f_0 k T_{\mathrm{s}} + \delta)} + \varepsilon_k \\ &= I_{\mathrm{m}} e^{j\delta} e^{j(2\pi f_0 k T_{\mathrm{s}})} + \varepsilon_k \end{aligned} \tag{2}$$

where N is the number of samples per cycle. To obtain δ, the Kalman filter is employed. The procedure of the Kalman filter is provided in Section II-A.

A. Kalman Filter

Kalman filter is a widely used tool for dealing with linear and nonlinear parameter estimation problems. Kalman filter can be used for parameter estimation from real-valued or complex data. Obviously, the complex implementation of the Kalman filter can provide simple modeling and lower computational complexity compared with real-valued ones [28], [29]. This section provides Kalman filter-based phase angle (δ) estimation from a new model of linear KF in the complex form that utilizes the complex current data given in (2). The dynamic model for the phase angle (δ) is represented by

$$x(k+1) = Ax(k) \tag{3}$$

where

$$x(k) = I_{\mathrm{m}} e^{j\delta} \tag{4}$$

$$A = 1. \tag{5}$$

The measurement equation is expressed by

$$z(k) = H(k)x(k) + \varepsilon_k \tag{6}$$

$$H(k) = e^{j(2\pi f_0 k T_{\mathrm{s}})}. \tag{7}$$

Kalman filter recursively calculates the unknown parameter $x(k)$ using the following expression:

$$\begin{aligned}\hat{x}(k|k) &= \hat{x}(k|k-1) + K(k)[z(k) - H(k)A\hat{x}(k-1|k-1)] \\ &= A\hat{x}(k-1|k-1) + K(k) \\ &\quad \times [z(k) - H(k)A\hat{x}(k-1|k-1)].\end{aligned} \tag{8}$$

In (8), $\hat{x}(k|k-1)$ is the estimate of unknown parameter and it is substituted by $A\hat{x}(k-1|k-1)$ which means the unknown parameter is predicted before the new sample of $z(k)$ is measured. The Kalman gain $K(k)$ is expressed by

$$K(k) = P(k|k-1) + H(k)\left[H(k)P(k|k-1)H^{\mathrm{trans}}(k) + R\right]^{-1}. \tag{9}$$

In (9), R is the observation noise variance $E[\varepsilon_k^2]$ and P is the prediction error covariance and it is calculated from the discrete-time Riccati equation as follows:

$$P(k+1|k) = A[P(k|k-1) - K(k)H(k)P(k|k-1)]A^{\mathrm{trans}}. \tag{10}$$

At each sampling point, the phase angle δ is calculated by

$$\delta(k) = \tan^{-1}\left(\frac{\mathrm{Imaginary}(\hat{x}(k))}{\mathrm{Real}(\hat{x}(k))}\right). \tag{11}$$

B. Proposed Discrimination Criterion

Considering δ_1 and δ_2 as the estimated phase angles of the current signals measure med by CT1 and CT2, respectively, the PDC is introduced by

$$\mathrm{PDC}(\delta_1, \delta_2) = \frac{|\delta_1 - \delta_2|}{\pi}. \tag{12}$$

Note that in (12), PDC is updated sample by sample. In general, the calculation of PDC is started when a change is detected in the differential protection relay. The different ranges of PDC under different circumstances are discussed in the following.

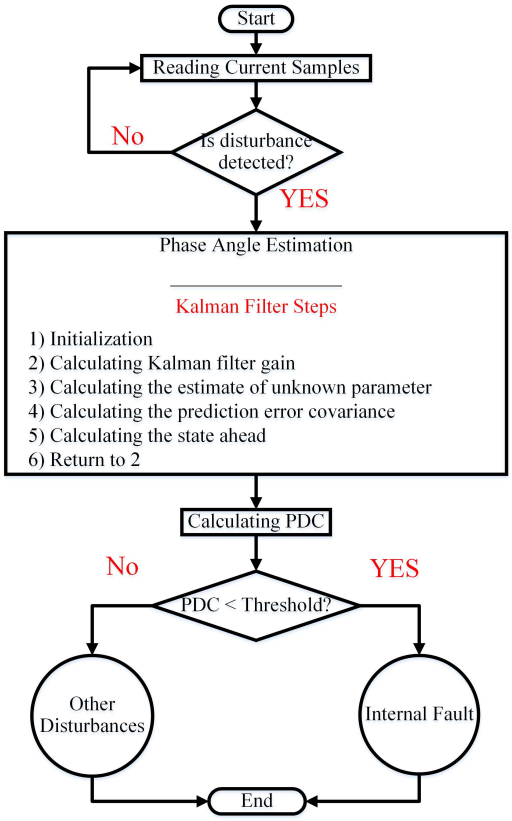

Fig. 1. Proposed algorithm flowchart.

III. Proposed Method Implementation

Fig. 1 shows the steps of the proposed algorithm including phase angle estimator and PDC calculations. The following steps are applied for internal fault identification.

1) *Reading Current Samples:* The samples are acquired from CTs and checked if a disturbance has happened. The proposed index performs its analysis after the differential current signal becomes greater than a threshold. If the differential current ($|I_{\mathrm{CT},1} - I_{\mathrm{CT},2}|$) signal triggers the operating current of the differential relay, then the signals of both CTs will be sent to the algorithm. The disturbance given in Fig. 1, is defined as the differential current signal that triggers the operating current of the differential relay. Here, the disturbance is selected if the differential current becomes greater than 10% of the nominal current.
2) *Applying Kalman filter:* Kalman filter is applied as follows:
   a) initializing the state variable and the prediction error covariance;
   b) calculating Kalman filter gain using (9);
   c) calculating the estimate of unknown parameters using (8);
   d) calculating the prediction error covariance using (10);
   e) calculating the state ahead using (3);
   f) return to b.
3) *Fundamental Phase Angle Estimation:* At each sampling point, the phase angle is calculated using (11).

TABLE II
SPECIFICATION OF THE INFLUENTIAL VARIABLES

Variable	Range
Switching Instance	[0,360°]
Fault Resistance	[0,10Ω]
Fault Inception Angle	[0,360°]
Fault Type	Single Phase to Ground Double Phase Double Phase to Ground Three Phase to Ground
Remnant Flux	[-60%,60%]
Noise Level	[30 dB, 60 dB]

TABLE III
VALUES OF PDC FOR DIFFERENT CONDITIONS IN THE FIRST QUARTER OF CYCLE AFTER DISTURBANCE OCCURRENCE

Condition	Minimum	Maximum
Internal Fault (with/without CT saturation)	0.01	0.1
Simultaneously Inrush and Internal Fault	0.06	0.24
External Fault (with/without CT saturation)	0.56	0.99
Inrush	0.45	0.99

4) *Calculating PDC:* The estimated fundamental phase angles are fed to (12) to calculate the distance between the phase angles. Eventually, a decision is made by comparing the PDC with a certain threshold to identify the internal faults.

IV. PERFORMANCE EVALUATION AND RESULTS DISCUSSION

This section is dedicated to the performance evaluation of the PDC. The evaluation is conducted with several simulations and experimentally recorded data.

A. Selecting Threshold

To obtain the threshold, 2000 scenarios are simulated according to several influential parameters given in Table II. The simulations scenarios contain 1000 scenarios for internal fault with/without CT saturation, 100 scenarios for simultaneously internal fault with inrush current, 600 scenarios for inrush current with/without remnant flux, and 300 scenarios for external fault with/without CT saturation. Table III shows the value of PDC in different conditions.

To obtain the threshold, the Otsu thresholding method is utilized [30]. Otsu thresholding method is implemented as follows.

Step1) A probability density function (PDF) is calculated for PDC for different conditions. In this investigation, the data are categorized as follows.

1) The first group of data contains internal fault (with/without CT saturation) and simultaneously inrush and internal fault which is designated as the fault condition.
2) The second group of data contains inrush and external fault (with/without CT saturation) which is designated as the nonfault condition.

Step2) A normal function-based curve should be fit for each case (fault and nonfault conditions).

Step3) The intersection point of the PDFs obtained for the fault and nonfault cases is selected as the threshold value.

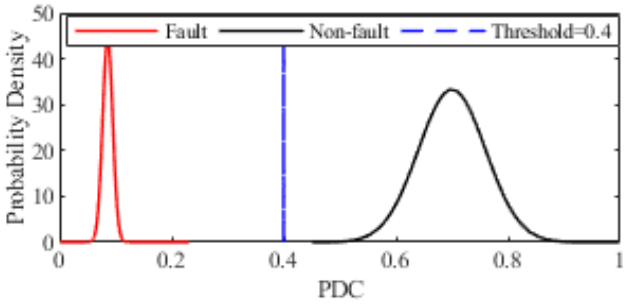

Fig. 2. PDFs for the PDC and the selected threshold.

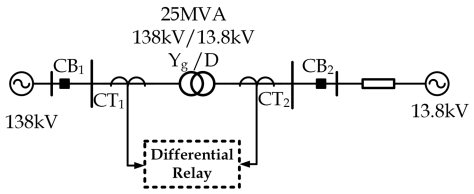

Fig. 3. Yg/D 138/13.8-kV transformer for simulation.

TABLE IV
SPECIFICATION OF THE TEST SYSTEM

Component	Specifications	Component	Specifications
138 kV source	R_+=7.1Ω, L_+=53.99mH	**13.8 kV source**	R_+=1.4Ω, L_+=5.6mH
	R_0=7.596Ω, L_0=115.45mH		R_0=1.498Ω, L_0=11.957mH
Transformer	R_1=0.908Ω, L_1=78.51mH	**Transmission line**	R_1=0.3101Ω, L_1=2.41mHl C1=26.8nF,
	R_2=0.0091Ω, L_2=0.7851mH		R_0=0.1437Ω L_0=11.45mH, C_0=5.635nF

Considering 2000 different fault and nonfault scenarios, as illustrated in Fig. 2, fortunately, the PDFs of the PDC for fault scenarios and nonfault scenarios do not intersect. Therefore, the threshold can be selected at any point in the range of 0.24–0.45. Here, the threshold is selected 0.4.

PDC is a normalized index that measures the distance between phase angles of the current signals. As a result, the threshold has no dependence on the power transformer or power system parameters.

B. Simulation Results

According to the test system given in Fig. 3, a Y_g/D 138/13.8-kV transformer is simulated in the MATLAB environment to provide different inrush and fault scenarios. The specifications of the test system are provided in Tables IV and V and Fig. 3. For CT modeling, saturation and hysteresis effects are modeled by using a nonlinear inductor in parallel with a resistance. Note that the resistance is used to model core loss power. The CTs are 10-VA class PX. The detailed specification of CTs is provided in Fig.4 and Table V.

Several scenarios including different internal fault scenarios with/without CT saturation, inrush current, and inrush current with internal fault, are generated to evaluate the performance of the proposed algorithm. The simulated scenarios are obtained considering different factors, which are tabulated

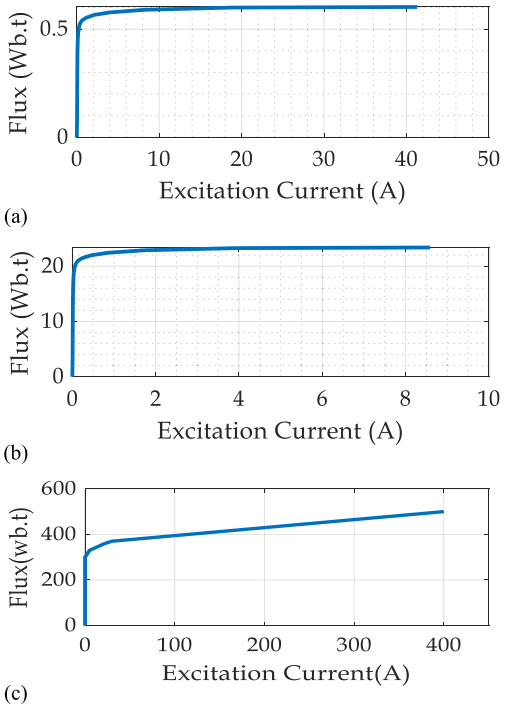

Fig. 4. Magnetization curves: (a) CT1; (b) CT2; and (c) power transformer.

TABLE V
SPECIFICATION OF THE CTS

	Primary Rated Current (A)	Secondary Rated Current (A)	Mean core length (cm)	Cross section area (mm^2)	Winding resistance (Ω)
CT1	100	5	42.5	30	2.3
CT2	1200	5	106	97	7.2

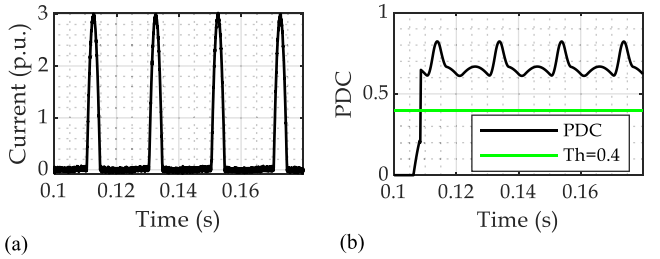

Fig. 5. Performance of the PDC for inrush current: (a) current signal and (b) PDC.

in Table II. It should be noted that the signals are recorded at 2 kHz (40 samples per cycle considering $f_0 = 50$ Hz).

1) Inrush Current: Fig. 5(a) shows a magnetization inrush current that is generated by transformer energization at $t = 0.105$ s. According to Fig. 5(b), the PDC immediately crosses the threshold (after 3.4 ms) and as a result, the PDC does not maloperate during inrush current.

As a different inrush case, a magnetization current with 60% residual flux is generated by energization of the power transformer at $t = 0.104$ s. Fig. 6(b), the PDC can identify such inrush current as well in less than a quarter of a cycle.

In general, the PDC experiences significant variations because the inrush current does not fit on a sinusoidal waveform such as (1) and, therefore, the phase angle of

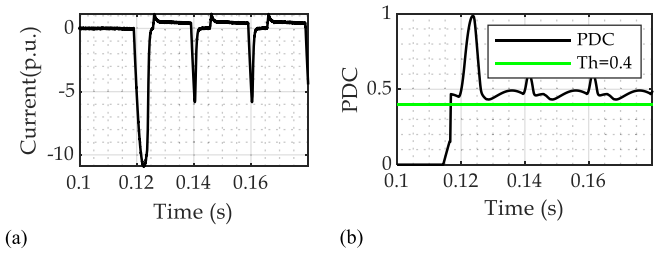

Fig. 6. Performance of the PDC for inrush current with residual flux: (a) current signal and (b) PDC.

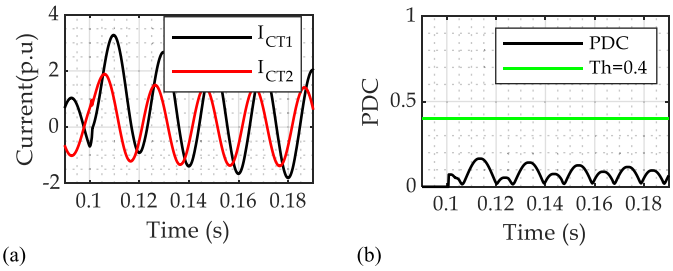

Fig. 7. Performance of the PDC for simulated internal fault scenario: (a) current signals and (b) PDC.

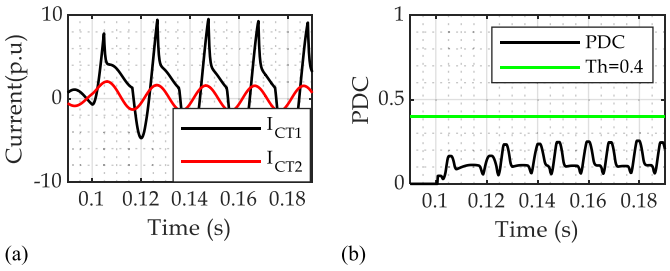

Fig. 8. Performance of the PDC for simulated internal fault scenario in presence of CT saturation: (a) current signals and (b) PDC.

the inrush current and consequently the PDC significantly changes.

2) Internal Fault Current: Fig. 7 provides the performance of the PDC for an internal fault on 15% of the star side of the power transformer winding which is initiated at $t = 0.1$ s. As illustrated in Fig. 7(b), the PDC does not cross the threshold after disturbance and it means the internal fault is identified.

Also in the case of internal fault accompanied by CT saturation, Fig. 8(b) shows the PDC can successfully recognize the internal fault.

Generally, in the case of an internal fault with/without CT saturation, due to the minor distance of the phase angles, the PDC does not cross the threshold. As a result, the PDC can effectively identify the internal fault even in the case of CT saturation.

3) Internal Fault During Transformer Energization: Transformer energization with an existing internal fault may lead to maloperation of the differential. Such a circumstance is generated by transformer energization at $t = 0.106$ s with a 15% fault in the star side of the power transformer. As shown in Fig. 9(b), the PDC can detect the internal fault. In the case of transformer energization with an internal fault, the faulty phase has more similarity to a sinusoidal current as a result,

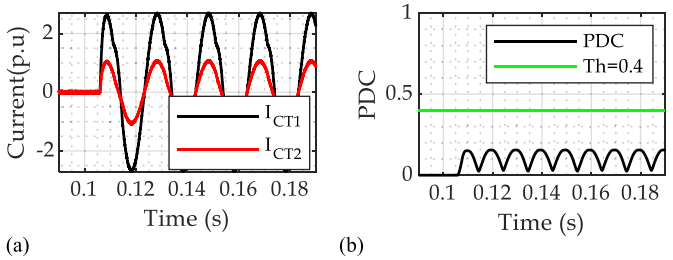

Fig. 9. Performance of the PDC for transformer energization with internal fault: (a) current signal and (b) PDC.

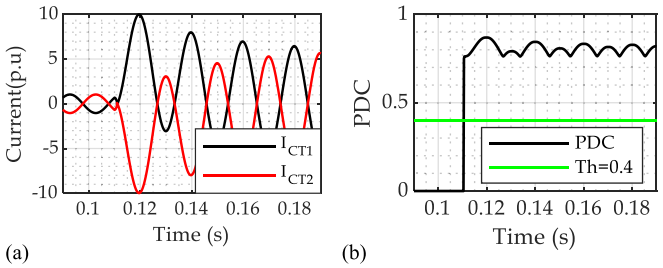

Fig. 10. Performance of the PDC for simulated external fault scenario: (a) current signals and (b) PDC.

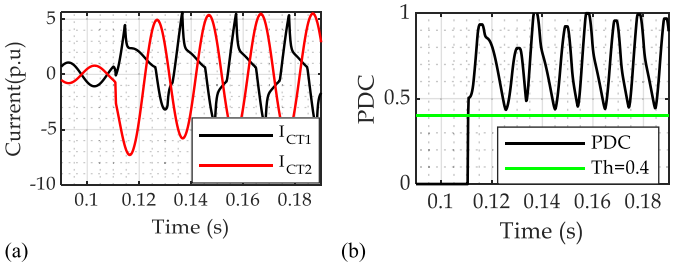

Fig. 11. Performance of the PDC for external fault with CT saturation: (a) current signal and (b) PDC.

the phase angle variations and consequently the PDC is much lower than the threshold.

4) External Fault: Figs. 10 and 11 show the performance of the PDC under external fault currents. In both cases of external fault given in Figs. 10 and 11, due to significant variation of the phase angle, the PDC crosses the threshold almost after 4 ms. Therefore, the PDC does not experience maloperation during external fault even in the case of CT saturation.

C. Performance Validation Using Experimental Recorded Signals

The experimental setup which is shown in Fig. 12 is provided to generate some experimental fault and inrush current signals. The experimental setup contains a power transformer with 6-kVA nominal apparent power. The power transformer operates at 50 Hz, with a voltage level of 330/330 V. The power transformer has different access terminals of the windings for recording internal faults. The CTs are "Chauvin Arnoux-France C113" model. The specifications of these CTs are provided in Table VI.

Considering transformer specification, the maximum load current is about 10.5 A. Considering current limitations for the sake of laboratory protection, the inrush and fault currents

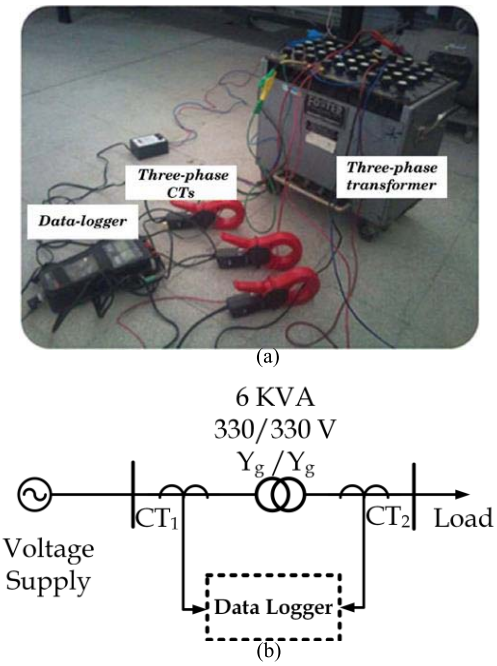

Fig. 12. (a) Experimental setup for generating fault and inrush currents and (b) single diagram of the experimental setup.

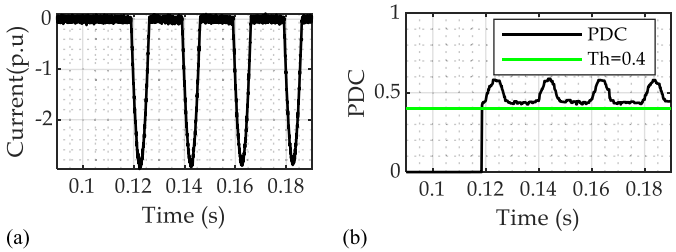

Fig. 13. Performance of the PDC for transformer energization: (a) current signal and (b) PDC.

do not exceed three or four times the nominal current. Even considering fault current 42 A (4 × 10.5 A), the current is still very lower than the nominal current of the CTs. As a result, CTs can be considered an ideal ampere meter.

The internal fault is applied by manually shorting the terminals. Inrush current is also generated by randomly switching the transformer. Of course in some switching angles, the inrush current may not be seen. Nevertheless, several inrush and fault signals are generated and recorded considering 128-μs sampling time for the data logger. In the following, some of the experimental scenarios are investigated.

According to Fig. 13, the PDC identifies the inrush current in almost 3 ms after transformer energization. In the case of internal fault shown in Fig. 14, the PDC has low value owning to low variation and minimum distance of phase angle of currents. On the contrary, as shown in Fig. 15, in the case of external fault, the PDC has a large value due to the distance of the phase angles of the current signals. In general, the proposed method requires only 3–4-ms data for reaching a reliable decision. Eventually, the results indicate that the PDC has noise sensitivity.

TABLE VI
SPECIFICATIONS OF THE CTS USED IN EXPERIMENTAL SETUP

Rated Current	1000				
Ratio	1000/1				
Primary current	1mA .. 100 mA	100 mA .. 1 A	1 A .. 10 A	10 A .. 100 A	100 A .. 1200 A
% Accuracy of output signal	≤ 3 % +5 μA	≤ 2 % +3 μA	≤ 1 %	≤ 0.5 %	≤ 0.3 %
Phase shift	Not Specified	Not Specified	≤ 2°	≤ 1°	≤ 0.7°
Maximum Operating Voltage	600 V (RMS)				
Load impedance	1 Ω				
Load Influence (1 Ω … 5 Ω)	< 0.1 % on measurement < 0.2° on phase				
Influence of conductor position in jaws	≤ 0.1 % of output signal for frequencies ≤ 400 Hz				
Influence of adjacent conductor	≤ 0.5 mA / A at 50 Hz				

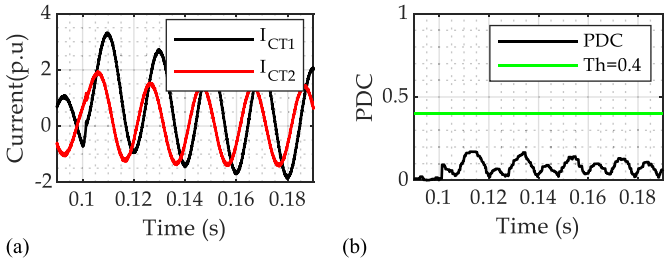

Fig. 14. Performance of the PDC for experimentally recorded internal fault condition: (a) current signals and (b) PDC.

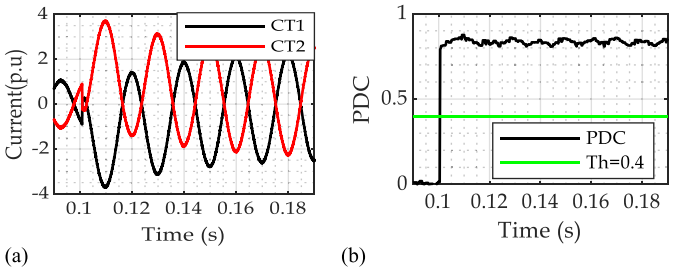

Fig. 15. Performance of the PDC for experimentally recorded external fault condition: (a) current signals and (b) PDC.

D. Performance Evaluation Using Field Recorded Data

This section is dedicated to evaluating the performance of the proposed index using recorded field data of a power transformer differential. The recorded data belong to a 15-MVA Yg/Δ power transformer operating at voltage level 33/11 kV. The transformer is part of the distribution grid of an oil company. The transformer is provided with a numerical differential protection scheme that is able to record data with a sampling rate of 20 samples/cycle and can memorize the event for 50 consecutive cycles. The power transformer's protection scheme utilizes CTs with 300/5 and 900/5 turn ratios for high and low voltage sides, respectively. The CTs are 10-VA class 5P10.

Fig. 16 shows a fault at phase C in the high voltage side of the power transformer. The fault location is at the terminal of the transformer and due to the high level of current, the CT in the high voltage side of the power transformer has become saturated. The signals of both CTs are applied to the

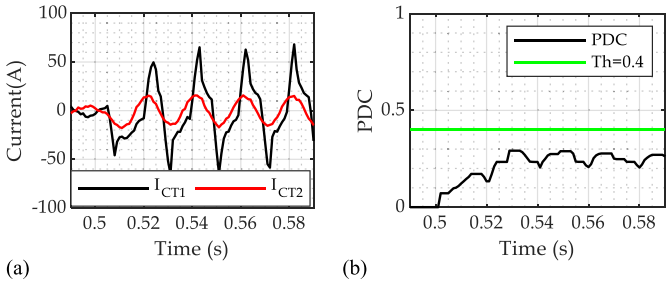

Fig. 16. Performance of the PDC for field recorded scenario of internal fault accompanied by CT saturation: (a) current signals and (b) PDC.

proposed algorithm. Nevertheless, as can be seen in Fig. 16, the proposed index has correctly identified the internal fault even in the presence of CT saturation.

E. Performance Comparison State-of-the-Art Algorithms

This section is dedicated to performance comparison between the PDC and state-of-the-art algorithms. In the following, some of the most recent algorithms for discrimination of internal faults from inrush currents are briefly described.

1) Kurtosis Method (KM) (see [23]): In [23], a method based on kurtosis was proposed that discriminated between inrush and internal fault in power transformers through the distribution characteristics of differential current. The distribution characteristics are obtained for one cycle data. According to the distribution characteristics, three kurtosis-based indices were introduced for distinguishing inrush currents from internal fault currents.

2) Discrete Fréchet Distance Method (DFDM) (see [24]): In [24], a similarity-based algorithm established on the DFDM has been presented. The DFD algorithm compares currents of CTs on both sides of the transformer. The DFD method utilizes a normalized signal and thus requires half-cycle cycle data to perform the normalization. Afterward, the DFD algorithm employs a quarter of the cycle to perform the calculation.

3) Improved Kurtosis Method (IKM) (see [27]): In [27], a kurtosis-based method so-called (IKM) was designed that distinguishes internal faults from inrush currents using twofold indices. The first index was designed to discriminate between inrush current and fault, while the second index was designed

TABLE VII

SPECIFICATIONS OF THE SELECTED ALGORITHMS FOR PERFORMANCE COMPARISON AND PROPOSED METHOD

	Method 1 (Ref.[23])	Method 2 (Ref.[24])	Method 3 (Ref.[27])	Proposed Method
Extra index for CT saturation detection	No	No	Yes	No
Operation during CT saturation	Yes	Yes	Yes	Yes
Dependency of threshold to the power system's variations	No	No	No	No
Data requirement	1 Cycle	(1/2) cycle	(1/4) cycle	Sample by Sample
Complexity	Medium	Medium	High	Low

TABLE VIII

TIME DELAY COMPARISON OF PROPOSED METHOD AND OTHER ALGORITHMS (DELAYS ARE IN ms)

		Method 1 (Ref.[23])	Method 2 (Ref.[24])	Method 3 (Ref.[27])	Proposed Method
Internal Faults	Minimum	18.1	10.2	4.4	3.6
	Average	19.3	12.7	4.8	4.1
	Maximum	21.9	14.9	5.5	4.4
Inrush	Minimum	20.1	10.3	4.8	3.3
	Average	23.5	13.2	5.9	3.7
	Maximum	28.8	15.6	8.2	4.1

to deal with internal fault identification in the presence of CT saturation. Unlike [23], this method utilizes an analytical formulation from the current signal considering the effect of the decaying dc component.

Table VII briefly shows the specifications of the selected methods from [23], [24], and [27] and the PDC. Table VIII provides the time delays for 500 internal faults including fault without CT saturation, fault with CT saturation, and minor fault (i.e., 10%–15% shorted winding) with transformer energization. Note that all methods have correctly identified these scenarios. According to Table VIII, the PDC has the lowest time delay compared with other algorithms in the detection of internal faults. According to Table VII, it can be concluded that since the PDC has a recursive nature that updates sample by sample, it requires very low memory compared with other algorithms.

Also, Table VIII provides the time delays for 500 inrush currents. All methods have correctly identified all 500 scenarios. According to Table VIII, Methods 1 and 2 have the highest time delay. Also, compared with Method 3, due to the recursive nature of the proposed method, the PDC reaches correct identification with the lowest time delay.

Comparing the results in Tables VII and VIII, it is concluded that the time delays are in accordance with the required window of data. However, both in internal fault scenarios and inrush currents, references [23], [24], and [27] experience higher delays. The higher delays are mostly observed during deep CT saturation, inrush current with high remnant flux. Note that references [23], [24], and [27] are only able to deal with discrimination internal fault from inrush currents. However, the PDC can deal with external faults as well. In general, the results reveal that the PDC can discriminate the internal fault, and also it can provide immunity against inrush and external fault currents considering different challenging scenarios.

V. CONCLUSION

Inrush current may threaten the performance of the power transformer differential protection and consequently leads to maloperation in power transformer. In this article, an algorithm based on a complex Kalman filter was developed to distinguish internal faults from inrush currents. The presented algorithm was founded on the distance between the phase angles of both CTs' currents. The PDC discriminated the internal faults from inrush and the external fault currents considering the fact that during an internal fault, the phase angles of both CTs are almost constant and in phase, during the external fault and inrush currents, the phase angles of both CTs have notable distance. Performance validation was conducted using several simulation and experimental data. From several evaluations, it was concluded the PDC can detect internal faults even in the case of CT saturation. Moreover, the PDC does not experience maloperation during inrush and external fault currents. Also, the PDC can successfully detect internal faults during transformer energization. The proposed method has low response delay in most cases. In addition, the proposed method can accurately operate in noisy conditions. Therefore, the proposed method can be applied for the discrimination of internal faults and inrush currents.

REFERENCES

[1] S. H. Horowitz and A. G. Phadke, *Power System Relaying*, 4th ed. Nashville, TN, USA: Wiley, 2013.

[2] M. E. H. Golshan, M. Saghaian-nejad, A. Saha, and H. Samet, "A new method for recognizing internal faults from inrush current conditions in digital differential protection of power transformers," *Electr. Power Syst. Res.*, vol. 71, no. 1, pp. 61–71, Sep. 2004.

[3] S. A. Saleh and M. A. Rahman, "Modeling and protection of a three-phase power transformer using wavelet packet transform," *IEEE Trans. Power Del.*, vol. 20, no. 2, pp. 1273–1282, Apr. 2005.

[4] G. Sivanagaraju, S. Chakrabarti, and S. C. Srivastava, "Uncertainty in transmission line parameters: Estimation and impact on line current differential protection," *IEEE Trans. Instrum. Meas.*, vol. 63, no. 6, pp. 1496–1504, Jun. 2014.

[5] A. Cataliotti *et al.*, "Compensation of nonlinearity of voltage and current instrument transformers," *IEEE Trans. Instrum. Meas.*, vol. 68, no. 5, pp. 1–11, May 2018.

[6] A. J. Collin, A. D. Femine, D. Gallo, R. Langella, and M. Luiso, "Compensation of current transformers' nonlinearities by tensor linearization," *IEEE Trans. Instrum. Meas.*, vol. 68, no. 10, pp. 3841–3849, Oct. 2019.

[7] Y.-P. Tsai, K.-L. Chen, Y.-R. Chen, and N. Chen, "Multifunctional coreless Hall-effect current transformer for the protection and measurement of power systems," *IEEE Trans. Magn.*, vol. 63, no. 3, pp. 557–565, Mar. 2014.

[8] Y. C. Kang, B. E. Lee, and S. H. Kang, "Transformer protection relay based on the induced voltages," *Int. J. Electr. Power Energy Syst.*, vol. 29, no. 4, pp. 281–289, May 2007.

[9] M. Mostafaei and F. Haghjoo, "Flux-based turn-to-turn fault protection for power transformers," *IET Gener., Transmiss. Distrib.*, vol. 10, no. 5, pp. 1154–1163, Apr. 2016.

[10] Z. Moravej, D. N. Vishwakarma, and S. P. Singh, "Application of radial basis function neural network for differential relaying of a power transformer," *Comput. Electr. Eng.*, vol. 29, no. 3, pp. 421–434, May 2003.

[11] M. Tripathy, R. P. Maheshwari, and H. K. Verma, "Application of probabilistic neural network for differential relaying of power transformer," *IET Gener., Transmiss. Distrib.*, vol. 1, no. 2, p. 218, 2007.

[12] H. Balaga, N. Gupta, and D. N. Vishwakarma, "GA trained parallel hidden layered ANN based differential protection of three phase power transformer," *Int. J. Electr. Power Energy Syst.*, vol. 67, pp. 286–297, May 2015.
[13] A. Wiszniewski and B. Kasztenny, "A multi-criteria differential transformer relay based on fuzzy logic," *IEEE Trans. Power Del.*, vol. 10, no. 4, pp. 1786–1792, Oct. 1995.
[14] M.-C. Shin, C.-W. Park, and J.-H. Kim, "Fuzzy logic-based relaying for large power transformer protection," *IEEE Trans. Power Del.*, vol. 18, no. 3, pp. 718–724, Jul. 2003.
[15] M. Gomez-Morante and D. W. Nicoletti, "A wavelet-based differential transformer protection," *IEEE Trans. Power Del.*, vol. 14, no. 4, pp. 1351–1358, Oct. 1999.
[16] M. M. Eissa, "A novel digital directional transformer protection technique based on wavelet packet," *IEEE Trans. Power Del.*, vol. 20, no. 3, pp. 1830–1836, Jul. 2005.
[17] S. A. Saleh, B. Scaplen, and M. A. Rahman, "A new implementation method of wavelet-packet-transform differential protection for power transformers," *IEEE Trans. Ind. Appl.*, vol. 47, no. 2, pp. 1003–1012, Mar./Apr. 2011.
[18] D. Guillén, H. Esponda, E. Vázquez, and G. Idárraga-Ospina, "Algorithm for transformer differential protection based on wavelet correlation modes," *IET Gener., Transmiss. Distrib.*, vol. 10, no. 12, pp. 2871–2879, Sep. 2016.
[19] A. Roy, D. Singh, R. K. Misra, and A. Singh, "Differential protection scheme for power transformers using matched wavelets," *IET Gener., Transmiss. Distrib.*, vol. 13, no. 12, pp. 2423–2437, Jun. 2019.
[20] E. Ali, A. Helal, H. Desouki, K. Shebl, S. Abdelkader, and O. P. Malik, "Power transformer differential protection using current and voltage ratios," *Electr. Power Syst. Res.*, vol. 154, pp. 140–150, Jan. 2018.
[21] E. Ali, O. P. Malik, S. Abdelkader, A. Helal, and H. Desouki, "Experimental results of ratios-based transformer differential protection scheme," *Int. Trans. Electr. Energy Syst.*, vol. 29, no. 11, Nov. 2019, Art. no. e12114.
[22] E. Ali, O. P. Malik, A. Knight, S. Abdelkader, A. Helal, and H. Desouki, "Ratios-based universal differential protection algorithm for power transformer," *Electr. Power Syst. Res.*, vol. 186, Sep. 2020, Art. no. 106383.
[23] L. L. Zhang, Q. H. Wu, T. Y. Ji, and A. Q. Zhang, "Identification of inrush currents in power transformers based on higher-order statistics," *Electr. Power Syst. Res.*, vol. 146, pp. 161–169, May 2017.
[24] H. Weng, S. Wang, X. Lin, Z. Li, and J. Huang, "A novel criterion applicable to transformer differential protection based on waveform sinusoidal similarity identification," *Int. J. Electr. Power Energy Syst.*, vol. 105, pp. 305–314, Feb. 2019.
[25] H. Weng, S. Wang, Y. Wan, X. Lin, Z. Li, and J. Huang, "Discrete Fréchet distance algorithm based criterion of transformer differential protection with the immunity to saturation of current transformer," *Int. J. Electr. Power Energy Syst.*, vol. 115, Feb. 2020, Art. no. 105449.
[26] T. Zheng, T. Huang, Y. Ma, Z. Zhang, and L. Liu, "Histogram-based method to avoid maloperation of transformer differential protection due to current-transformer saturation under external faults," *IEEE Trans. Power Del.*, vol. 33, no. 2, pp. 610–619, Apr. 2018.
[27] M. Tajdinian, M. Allahbakhshi, A. Bagheri, H. Samet, P. Dehghanian, and O. P. Malik, "An enhanced sub-cycle statistical algorithm for inrush and fault currents classification in differential protection schemes," *Int. J. Electr. Power Energy Syst.*, vol. 119, Jul. 2020, Art. no. 105939.
[28] G. Wang, S. S. Ge, R. Xue, J. Zhao, and C. Li, "Complex-valued Kalman filters based on Gaussian entropy," *Signal Process.*, vol. 160, pp. 178–189, Jul. 2019.
[29] A. G. Phadke and J. S. Thorp, *Computer Relaying for Power Systems*, 2nd ed. Hoboken, NJ, USA: Wiley, 2009.
[30] N. Otsu, "A threshold selection method from gray-level histograms," *IEEE Trans. Syst., Man, Cybern., Syst.*, vol. SMC-9, no. 1, pp. 62–66, Feb. 1979.

Mohsen Tajdinian received the Ph.D. degree in electrical engineering from Shiraz University, Shiraz, Iran, in 2020.

His main research interests are power system protection and power system stability.

Haidar Samet (Member, IEEE) received the Ph.D. degree in electrical engineering from the Isfahan University of Technology, Isfahan, Iran, in 2008.

He is currently a Professor with Shiraz University, Shiraz, Iran, and a Post-Doctoral Researcher with the Eindhoven University of Technology, Eindhoven, The Netherlands. His main research interest is application of DSP techniques in power systems, especially protection and power quality.

Ziad M. Ali received the B.Sc. and M.Sc. degrees in electrical engineering from the Faculty of Engineering, Assiut University, Assiut, Egypt, in 1998 and 2003, respectively, and the Ph.D. degree from Kazan State Technical University, Kazan, Tatarstan, Russia, in 2010.

He worked as a Demonstrator with the Aswan Faculty of Engineering, South Valley University, Aswan, Egypt. He worked as an Assistant Lecturer and an Assistant Professor, from 2011 to 2016, with the Aswan Faculty of Engineering, Aswan, a Visitor Researcher with the Power System Laboratory, Kazan State Energy University, Kazan, from 2012 to 2013, and a Visitor Researcher with the Power System Laboratory, College of Engineering, University of Padova, Padua, Italy, from 2013 to 2014. He is currently working as an Associate Professor with the Electrical Department, Aswan Faculty of Engineering, Aswan University, Aswan, and also with the College of Engineering at Wadi Addawasir, Prince Sattam Bin Abdulaziz University, Al-Kharj, Saudi Arabia. His research interests include power system analysis, flexible alternative current transmission systems (FACTS), optimization, renewable energy analysis, smart grid, and material science.